Petroleum Research 11 (2026) 995–1007

Contents lists available at ScienceDirect

Petroleum Research

journal homepage: http://www.keaipublishing.com/en/journals/petroleum-research/

Full Length Article

A new model of predicting the optimal mud density for maximizing the open-hole extension capacity in offshore extended-reach horizontal well drilling

Xuyue Chen [a,b,*], Gengchen Li [a,b], Qiqi Yang [a,b], Jin Yang [a,b], Deli Gao [a,b], Qinyi He [b,c]

[a] Hainan Institute of China University of Petroleum (Beijing), Sanya, Hainan, 572000, China
[b] MOE Key Laboratory of Petroleum Engineering, China University of Petroleum (Beijing), Beijing, 102249, China
[c] PetroChina Tarim Oilfield Company, Korla, 841000, China

ARTICLE INFO

Article history:
Received 25 July 2025
Received in revised form
25 January 2026
Accepted 26 January 2026
Available online 29 January 2026

Keywords:
Offshore drilling
Extended-reach horizontal wells
Open-hole extension capacity
Optimal mud density

ABSTRACT

The pressure fluctuation caused by the axial movement of the string easily causes the bottomhole pressure to exceed the safe pressure window, which seriously restricts the horizontal open-hole extension capacity (OHEC) of the offshore extended-reach horizontal wells (ERHWs). In this work, in order to improve the horizontal OHEC for ERHWs, an optimal mud density model in extended-reach horizontal drilling (ERHD) was established based on the prediction and analysis of horizontal OHEC of ERHWs under string tripping operations. The results show that with the increase of mud density, the horizontal OHEC has a trend of first increasing and then decreasing in both tripping operations and casing tripping operations, and there exists an optimal mud density to maximize the horizontal OHEC. The optimal mud density of the two operations is obtained when the horizontal OHEC of the two operations is equal, and it is positively correlated with pull out of hole (POOH) speed, diameter of the wellbore and drill string, whereas it is negatively correlated with diameter of the casing and casing running speed. Controlling the tripping speed and optimizing the rheological properties are crucial to improve the horizontal OHEC. This model can provide scientific basis for optimization design of ERHD and the improvement of horizontal OHEC of ERHWs.

© 2026 Chinese Petroleum Society. Publishing services by Elsevier B.V. on behalf of KeAi Communications Co. Ltd. This is an open access article under the CC BY-NC-ND license (http://creativecommons.org/licenses/by-nc-nd/4.0/).

1. Introduction

To ensure the stable supply of global oil and gas resources, the exploration and development of offshore oil and gas resources have garnered significant attention (Melikoglu, 2018; Wada et al., 2018; Wen et al., 2023; Chen et al., 2025). Notably, the progress in ERHWs and cluster ERHWs has driven remarkable advancements in offshore oil and gas development. These technologies play a crucial role in the efficient development of marginal oilfields, utilization of clean energy, resolution of maritime use conflicts, expansion of platform coverage, and reduction of oil and gas development costs (Lan et al., 2018; Chen et al., 2020, 2022). However, compared to onshore fields, offshore drilling often faces challenges such as significant water depths, soft and under-compacted formations, which narrow the safe mud weight window (SMWW) and complicate mud density optimization (Rocha et al., 2003a, 2003b; Willson et al., 2003; Yin et al., 2023). If the mud density is too low, it can lead to wellbore instability and overflow (Suo et al., 2024); if it is too high, it may cause lost circulation. Therefore, to ensure the safety of drilling operations in offshore ERHWs, a reasonable mud density must be determined to prevent downhole accidents (Li et al., 2020; Song et al., 2016), the mud density is directly related to OHEC of ERHWs. During tripping operations, the axial motion of the drill string induces pressure fluctuations, which can easily cause the bottomhole pressure to exceed the safety pressure window (He et al., 2016), which typically results in a reduction of OHEC in ERHWs. Field practices indicate that most downhole accidents, such as blowouts, overflows, wellbore collapse, and well leakage, often occur during tripping operations (Tang et al., 2016), with over 25% of blowout caused by excessive POOH speed of string generating suction

* Corresponding author.
E-mail addresses: chenxuyue@cup.edu.cn, chenxuyue2011@163.com (X. Chen).
Peer review under the responsibility of Editorial Office of Petroleum Research.

https://doi.org/10.1016/j.ptlrs.2026.01.016
2096-2495/© 2026 Chinese Petroleum Society. Publishing services by Elsevier B.V. on behalf of KeAi Communications Co. Ltd. This is an open access article under the CC BY-NC-ND license (http://creativecommons.org/licenses/by-nc-nd/4.0/).

pressure (Islam et al., 2017). To further enhance the OHEC of ERHWs and reach deeper underground targets, it is necessary to establish a method for optimizing drilling fluid density based on the OHEC during string tripping operations.

Mason and Judzis (1998) proposed that the extension limit of ERHWs can be divided into mechanical limit and wellbore stability limit. Rocha et al. (2003a,b) subsequently identified annular pressure loss as a key factor limiting the extension capacity of ERHWs. Gao et al. (2009) systematically introduced the theoretical concept of the extension limit for ERHWs and developed an open-hole extension limit model. Livescu et al. (2014) investigated the open-hole section of ERHWs, identifying frictional torque and strength as key factors affecting the extension limit of drill string. Huang et al. (2015) developed a mechanical model for drill string buckling behavior in horizontal wells and proposed criteria for determining and calculating mechanical extension limit. Chen and Gao (2016, 2018) provided a calculation model for the open-hole extension limit of ERHWs targeting deep water environment and analyzed the impacts of formation anisotropy. Li et al. (2017a) optimized the open-hole extension limit model for ERHWs, proposing optimization design principles and control methods under subjective and objective constraints, while also optimizing mud flow rate. Gao et al. (2019) suggested that the proper use of drilling fluid density can also enhance the extension limits during the drilling of ERHWs. Li et al. (2022) improved the hydraulic extension limit of ERHWs by optimizing the string size, achieving an enhancement of 18.47–22.69%. Shi et al. (2023) developed a dynamic model of drill string equipped with vibration dampers during ERHD and conducted research on optimizing excitation parameters and installation positions. Wang et al. (2024) proposed using the maximum temperature endured by bottomhole assembly as a constraint to optimize the drilling extension limit for geothermal horizontal wells. Zhang et al. (2024) examined the relationship between wavy wellbore trajectories, open-hole extension limit, and production distribution patterns. However, none of these studies have deeply explored the optimization of mud density in ERHWs drilling. In this paper, in order to improve the horizontal OHEC for ERHWs, an optimal mud density model in ERHD was established based on the prediction and analysis of horizontal OHEC of ERHWs under string tripping operations. The model may provide a theoretical foundation for optimizing mud density and enhancing OHEC in ERHD.

2. Optimal mud density model in ERHD

During string tripping operations, pressure fluctuations caused by the axial movement of the string can easily exceed the range of the safe pressure window at the bottomhole, leading to complex downhole accidents such as overflow, well collapse, and lost circulation (see Fig. 1), which significantly reduces the horizontal OHEC in ERHD. The impact of drilling fluid density on OHEC in ERHD varies under different string tripping conditions. To enhance the extension capability in ERHD, it is necessary to establish an optimal drilling fluid density model for string tripping operations.

2.1. Model assumptions

The following assumptions were made in this study.

(1) The density of the mud in the annulus remains constant with changes in temperature and pressure.
(2) The effects of casing inner wall roughness, wellbore roughness, and string connections on annular pressure loss are neglected.
(3) The mud flow induced by pipe tripping is considered to be in a turbulent state (Li et al., 2024; Zhang, 2023).

Given that the maximum horizontal OHEC is determined by the dynamic balance of bottomhole pressure and wellbore stability conditions, the optimal mud density model is primarily derived from the constraints of bottomhole pressure dynamic balance and the SMWW.

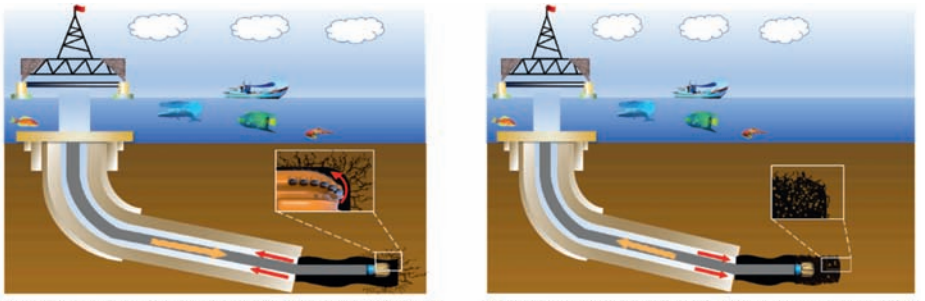
2.2. The predict model of OHEC during the operations of drilling

The transportation of cuttings in sections with large inclinations is challenging and can lead to the formation of a cuttings bed in ERHD. This phenomenon significantly impacts the annular pressure loss during circulation. If the bottomhole pressure during drilling is maintained below the formation fracture pressure, the OHEC can be assumed to increase continuously. The prediction model for the horizontal OHEC during drilling is described as follows (Li et al., 2017b):

$$L_{\mathrm{dri}} = \frac{0.00981\left(\rho_f - \rho_s C_s - \rho_m(1-C_s)\right)D_v - \Delta p_a}{(\Delta p/\Delta L)_h} \tag{1}$$

2.3. The predict model of OHEC during the operations of drill string tripping

During POOH operation, suction pressure is generated at the bottomhole. If the effective bottomhole pressure, defined as the mud hydrostatic pressure minus the suction pressure, falls below the formation pore pressure or the wellbore collapse pressure, a kick or wellbore collapse may occur (Siddiqi et al., 2016). To prevent kicks or wellbore collapse, the wellbore pressure must satisfy



(a) Wellbore collapse caused by suction pressure during POOH operation of string

(b) Wellbore lost circulation caused by surge pressure during run in hole operation of string

Fig. 1. Wellbore instability caused by pressure fluctuation under string tripping operation in ERHD.

the following conditions:

$$g\max(\rho_c,\rho_p)D_v \le g\rho_m D_v - p_{sc} \tag{2}$$

During run in hole (RIH) process, surge pressure is generated at the bottomhole. When the sum of the mud hydrostatic pressure and surge pressure exceeds the formation fracture pressure, lost circulation may occur. To prevent lost circulation, the bottomhole pressure must satisfy the following conditions:

$$g\rho_m D_v + p_{sx} \le g\rho_f D_v \tag{3}$$

Under tripping operations, Equations (2) and (3) can be reformulated to represent critical conditions.

$$\begin{cases} p_{sc} = g[\rho_m - \max(\rho_c,\rho_p)]D_v \\ p_{sx} = g\left(\rho_f - \rho_m\right)D_v \end{cases} \tag{4}$$

Generally, the suction pressure during POOH process and the surge pressure during RIH process occur in the vertical section, inclined section, and horizontal section of the ERHWs, respectively. The suction pressure and surge pressure can be expressed as:

$$\begin{cases} p_{sc} = \Delta p_{h-qz} + \int \Delta p_{qz}(\rho_m, L)\mathrm{d}L \\ p_{sx} = \Delta p_{h-xz} + \int \Delta p_{xz}(\rho_m, L)\mathrm{d}L \end{cases} \tag{5}$$

The suction pressure and surge pressure generated in the vertical section and inclined sections are:

$$\begin{cases} \int \Delta p_{qz}(\rho_m, L)\mathrm{d}L = \int_0^{L_v+L_{di}} \dfrac{2f_{qz}\rho_m v_{qz}^2}{D_o - D_{dp}}\mathrm{d}L \\ \int \Delta p_{xz}(\rho_m, L)\mathrm{d}L = \int_0^{L_v+L_{di}} \dfrac{2f_{xz}\rho_m v_{xz}^2}{D_o - D_{dp}}\mathrm{d}L \end{cases} \tag{6}$$

Annular friction coefficient can be expressed as:

$$\begin{cases} f_{qz} = \dfrac{a}{Re_{qz}^b} \\ f_{xz} = \dfrac{a}{Re_{xz}^b} \end{cases} \tag{7}$$

For the power-law fluid, the Reynolds number of the mud during tripping operation can be expressed as (Fan, 2014):

$$\begin{cases} Re_{qz} = \dfrac{12^{1-n}\rho_m\left(D_o - D_{dp}\right)^n v_{qz}^{2-n}}{K\left(\frac{2n+1}{3n}\right)^n} \times 10^{3-3n} \\ Re_{xz} = \dfrac{12^{1-n}\rho_m\left(D_o - D_{dp}\right)^n v_{xz}^{2-n}}{K\left(\frac{2n+1}{3n}\right)^n} \times 10^{3-3n} \end{cases} \tag{8}$$

In the case of a small annular clearance, the annular mud flow rate during tripping operation can be expressed as (Fan, 2014):

$$\begin{cases} v_{qz} = 1.5v_{ph}\left(\dfrac{D_{dp}^2}{D_o^2 - D_{dp}^2} + 0.5\right) \\ v_{xz} = 1.5v_{rh}\left(\dfrac{D_{dp}^2}{D_o^2 - D_{dp}^2} + 0.5\right) \end{cases} \tag{9}$$

By solving the system of Equations (4)–(6), the suction pressure and surge pressure caused by the horizontal section during the tripping process under the critical conditions ensuring wellbore stability can be obtained:

$$\begin{cases} \Delta p_{h-qz} = g[\rho_m - \max(\rho_c,\rho_p)]D_v \\ \quad - \int_0^{L_v+L_{di}} \dfrac{2f_{qz}\rho_m v_{qz}^2}{D_o - D_{dp}}\mathrm{d}L \\ \Delta p_{h-xz} = g\left(\rho_f - \rho_m\right)D_v \\ \quad - \int_0^{L_v+L_{di}} \dfrac{2f_{xz}\rho_m v_{xz}^2}{D_o - D_{dp}}\mathrm{d}L \end{cases} \tag{10}$$

The horizontal OHEC during POOH operation and RIH operation can be expressed respectively as:

$$\begin{cases} L_{h-qz} = \dfrac{\Delta p_{h-qz}}{\left(\frac{\Delta p_{h-qz}}{\Delta L}\right)} \\ L_{h-xz} = \dfrac{\Delta p_{h-xz}}{\left(\frac{\Delta p_{h-xz}}{\Delta L}\right)} \end{cases} \tag{11}$$

For turbulent flow conditions, the annular pressure loss gradient in the horizontal section during tripping operations can be expressed as:

$$\begin{cases} \dfrac{\Delta p_{h-qz}}{\Delta L} = \dfrac{2f_{qz}\rho_m v_{qz}^2}{D_o - D_{dp}} \\ \dfrac{\Delta p_{h-xz}}{\Delta L} = \dfrac{2f_{xz}\rho_m v_{xz}^2}{D_o - D_{dp}} \end{cases} \tag{12}$$

Substituting Equations (11) and (12) into Equation (10), it can be obtained:

$$\begin{cases} L_{h-qz} = \dfrac{gD_v\left(D_o - D_{dp}\right)}{2f_{qz}v_{qz}^2} - \dfrac{\int_0^{L_v+L_{di}} \frac{2f_{qz}\rho_m v_{qz}^2}{D_o - D_{dp}}\mathrm{d}L}{\frac{2f_{qz}\rho_m v_{qz}^2}{D_o - D_{dp}}} \\ \quad - \dfrac{1}{\rho_m}\dfrac{g\max(\rho_c,\rho_p)D_v\left(D_o - D_{dp}\right)}{2f_{qz}v_{qz}^2} \\ L_{h-xz} = \dfrac{1}{\rho_m}\dfrac{g\rho_f D_v\left(D_o - D_{dp}\right)}{2f_{xz}v_{xz}^2} \\ \quad - \dfrac{gD_v\left(D_o - D_{dp}\right)}{2f_{xz}v_{xz}^2} - \dfrac{\int_0^{L_v+L_{di}} \frac{2f_{xz}\rho_m v_{xz}^2}{D_o - D_{dp}}\mathrm{d}L}{\frac{2f_{xz}\rho_m v_{xz}^2}{D_o - D_{dp}}} \end{cases} \tag{13}$$

Let $A = -\frac{g\max(\rho_c,\rho_p)D_v(D_o-D_{dp})}{2f_{qz}v_{qz}^2}$, $B = \frac{g\rho_f D_v(D_o-D_{dp})}{2f_{xz}v_{xz}^2}$,then by differentiating L_{h-qz}、 L_{h-xz} with respect to the density ρ_m, it can be obtained:

$$\begin{cases} \dfrac{\mathrm{d}L_{h-qz}}{\mathrm{d}\rho_m} = -\dfrac{A}{\rho_m^2} \\ \dfrac{\mathrm{d}L_{h-xz}}{\mathrm{d}\rho_m} = -\dfrac{B}{\rho_m^2} \end{cases} \tag{14}$$

As $A<0$, $B>0$,thus $\frac{\mathrm{d}L_{h-qz}}{\mathrm{d}\rho_m}>0$, $\frac{\mathrm{d}L_{h-xz}}{\mathrm{d}\rho_m}<0$,the horizontal OHEC under the POOH operation will show an increasing trend, while the

horizontal OHEC under the RIH operation will show a decreasing trend. Therefore, there exists an optimal mud density that yields the maximum horizontal OHEC.

Let $L_{h-qz} = L_{h-xz}$, by simplifying above formulas can be obtained:

$$\frac{1}{f_{qz}v_{qz}^2}+\frac{1}{f_{xz}v_{xz}^2}=\frac{1}{\rho_m}\left[\frac{\rho_f}{f_{xz}v_{xz}^2}+\frac{\max(\rho_c,\rho_p)}{f_{qz}v_{qz}^2}\right] \tag{15}$$

Introduce the parameter for tripping, $\phi = v_{xz}/v_{qz}$ and combine Equations (7) and (8), then the ratio of the annular friction coefficient when RIH operation to that when POOH operation is:

$$\frac{f_{xz}}{f_{qz}}=\frac{a}{\mathrm{Re}_{xz}^b}\frac{\mathrm{Re}_{qz}^b}{a}=\begin{cases}\dfrac{v_{qz}^{2-n}}{v_{xz}^{2-n}}=\left(\dfrac{v_{xz}}{v_{qz}}\right)^{n-2}=\phi^{n-2}\ (\mathrm{Re}\le 2100)\\ \dfrac{v_{qz}^{2b-nb}}{v_{xz}^{2b-nb}}=\left(\dfrac{v_{xz}}{v_{qz}}\right)^{nb-2b}=\phi^{nb-2b}\ (\mathrm{Re}>2100)\end{cases} \tag{16}$$

Substituting Equation (16) into Equation (15) yields:

$$\begin{cases}\dfrac{\rho_f+\phi^{n-2}\max(\rho_c,\rho_p)}{\rho_m}=1+\phi^{n-2}\ (\mathrm{Re}\le 2100)\\ \dfrac{\rho_f+\phi^{nb-2b+2}\max(\rho_c,\rho_p)}{\rho_m}=1+\phi^{nb-2b+2}\ (\mathrm{Re}>2100)\end{cases} \tag{17}$$

After rearranging, the optimal mud density for combined tripping operations is obtained:

$$\rho_m=\begin{cases}\dfrac{\rho_f+\phi^{n-2}\max(\rho_c,\rho_p)}{1+\phi^{n-2}}\ (\mathrm{Re}\le 2100)\\ \dfrac{\rho_f+\phi^{nb-2b+2}\max(\rho_c,\rho_p)}{1+\phi^{nb-2b+2}},b=0.25-0.143\lg n\ (\mathrm{Re}>2100)\end{cases} \tag{18}$$

2.4. The operations of casing tripping

Similar to the tripping process, in the operations of casing tripping, the horizontal OHEC L_{h-st} during the casing pulling condition and the horizontal OHEC L_{h-xf} during the casing running condition can be expressed as (Xu et al., 2020):

$$\begin{cases}L_{h-st}=\dfrac{g[\rho_m-\max(\rho_c,\rho_p)]D_v}{\dfrac{2f_{st}\rho_m v_{st}^2}{D_o-D_{cp}}}-\dfrac{\int\Delta p_{st}(\rho_m,L)dL}{\dfrac{2f_{st}\rho_m v_{st}^2}{D_o-D_{cp}}}\\ L_{h-xf}=\dfrac{g\left(\rho_f-\rho_m\right)D_v}{\dfrac{2f_{xf}\rho_m v_{xf}^2}{D_o-D_{cp}}}-\dfrac{\int\Delta p_{xf}(\rho_m,L)dL}{\dfrac{2f_{xf}\rho_m v_{xf}^2}{D_o-D_{cp}}}\end{cases} \tag{19}$$

Among which:

$$\begin{cases}\int\Delta p_{st}(\rho_m,L)dL=\displaystyle\int_0^{L_v+L_{di}}\frac{2f_{st}\rho_m v_{st}^2}{D_o-D_{cp}}dL\\ \int\Delta p_{xf}(\rho_m,L)dL=\displaystyle\int_0^{L_v+L_{di}}\frac{2f_{xf}\rho_m v_{xf}^2}{D_o-D_{cp}}dL\end{cases} \tag{20}$$

Substitute Equation (20) into Equation (19):

$$\begin{cases}L_{h-st}=\dfrac{gD_v(D_o-D_{cp})}{2f_{st}v_{st}^2}-\dfrac{\int_0^{L_v+L_{di}}\dfrac{2f_{st}\rho_m v_{st}^2}{D_o-D_{cp}}dL}{\dfrac{2f_{st}\rho_m v_{st}^2}{D_o-D_{cp}}}\\ -\dfrac{1}{\rho_m}\dfrac{g\max(\rho_c,\rho_p)D_v(D_o-D_{cp})}{2f_{st}v_{st}^2}\\ L_{h-xf}=\dfrac{1}{\rho_m}\dfrac{g\rho_f D_v(D_o-D_{cp})}{2f_{xf}v_{xf}^2}-\dfrac{\int_0^{L_v+L_{di}}\dfrac{2f_{xf}\rho_m v_{xf}^2}{D_o-D_{cp}}dL}{\dfrac{2f_{xf}\rho_m v_{xf}^2}{D_o-D_{cp}}}\\ -\dfrac{gD_v(D_o-D_{cp})}{2f_{xf}v_{xf}^2}\end{cases} \tag{21}$$

Let $A'=-\frac{g\max(\rho_c,\rho_p)D_v(D_o-D_{cp})}{2f_{st}v_{st}^2}$, $B'=\frac{g\rho_f D_v(D_o-D_{cp})}{2f_{xf}v_{xf}^2}$,then by differentiating L_{h-st}、L_{h-xf} represent to the density ρ_m:

$$\begin{cases}\dfrac{dL_{h-st}}{d\rho_m}=-\dfrac{A'}{\rho_m^2}\\ \dfrac{dL_{h-xf}}{d\rho_m}=-\dfrac{B'}{\rho_m^2}\end{cases} \tag{22}$$

As $A'<0$, $B'>0$,therefore $\frac{dL_{h-st}}{d\rho_m}>0$, $\frac{dL_{h-xf}}{d\rho_m}<0$, Similar to the tripping operation, there exists an optimal mud density in casing tripping operations. The maximum horizontal OHEC can be achieved when this optimal mud density is used.

Let $L_{h-st} = L_{h-xf}$,by simplifying above formulas can be obtained:

$$\frac{1}{f_{st}v_{st}^2}+\frac{1}{f_{xf}v_{xf}^2}=\frac{1}{\rho_m}\left[\frac{\rho_f}{f_{xf}v_{xf}^2}+\frac{\max(\rho_c,\rho_p)}{f_{st}v_{st}^2}\right] \tag{23}$$

Introduce the parameters for casing tripping. $\eta = v_{xf}/v_{st}$, then the ratio of the annular friction coefficient when casing running operation to that when pulling operation is:

$$\frac{f_{xf}}{f_{st}}=\frac{a}{\mathrm{Re}_{xf}^b}\frac{\mathrm{Re}_{st}^b}{a}=\begin{cases}\dfrac{v_{st}^{2-n}}{v_{xf}^{2-n}}=\left(\dfrac{v_{xf}}{v_{st}}\right)^{n-2}=\eta^{n-2}\ (\mathrm{Re}\le 2100)\\ \dfrac{v_{st}^{2b-nb}}{v_{xf}^{2b-nb}}=\left(\dfrac{v_{xf}}{v_{st}}\right)^{nb-2b}=\eta^{nb-2b}\ (\mathrm{Re}>2100)\end{cases} \tag{24}$$

Substituting Equation (24) into Equation (23) yields:

$$\begin{cases}\dfrac{\rho_f+\eta^{n-2}\max(\rho_c,\rho_p)}{\rho_m}=1+\eta^{n-2}\ (\mathrm{Re}\le 2100)\\ \dfrac{\rho_f+\eta^{nb-2b+2}\max(\rho_c,\rho_p)}{\rho_m}=1+\eta^{nb-2b+2}\ (\mathrm{Re}>2100)\end{cases} \tag{25}$$

After rearranging, the optimal mud density for the casing tripping operation can be obtained:

$$\rho_m=\begin{cases}\dfrac{\rho_f+\eta^{n-2}\max(\rho_c,\rho_p)}{1+\eta^{n-2}}\ (\mathrm{Re}\le 2100)\\ \dfrac{\rho_f+\eta^{nb-2b+2}\max(\rho_c,\rho_p)}{1+\eta^{nb-2b+2}},b=0.25-0.143\lg n\ (\mathrm{Re}>2100)\end{cases} \tag{26}$$

2.5. Analysis of combined drilling operations

To further optimize the mud density, it is essential to consider both tripping and casing tripping operations when establishing a predictive model for the optimal mud density. According to field practice, the optimal mud density under tripping conditions is generally higher than under casing tripping conditions. There are two possible scenarios, where L_{h-qx} represents the horizontal OHEC during tripping operation, and L_{h-tf} represents the horizontal OHEC during casing tripping operations, ρ_{m-qx} represents the optimal drilling mud density during tripping operation, and ρ_{m-tf} represents the optimal drilling mud density during casing tripping operations.

(1) If the curve of L_{h-qx} does not intersect with the curve of L_{h-tf} and L_{h-qx} is always greater than L_{h-tf} (see Fig. 2), then the horizontal OHEC is solely controlled by the casing tripping conditions. In this case, the maximum value of the curve L_{h-tf} represents the maximum horizontal OHEC, and the ρ_{m-tf} value represents the optimal mud density.
(2) If the curve of L_{h-qx} intersects with the curve of L_{h-tf}, there are four possible scenarios:

Scenario a: There exists an optimal mud density, denoted as $\rho_{m-com-optimal}$, which is jointly controlled by the RIH operation and the casing pulling operation (see Fig. 3(a)).

Scenario b: There exists an optimal mud density, denoted as $\rho_{m-com-optimal}$, which is jointly controlled by the POOH operation and the casing running operation (see Fig. 3(b)).

Scenario c: The optimal mud density is the one from the casing tripping operation. In this scenario, there is a maximum mud density, above which the horizontal OHEC under the combined operation will significantly decrease. This maximum density is controlled by the RIH operation and the casing running operation. The recommended mud density ranges from $\rho_{m-com-optimal}$ to $\rho_{m-com-max}$ (see Fig. 3(c)).

Scenario d: The optimal mud density is the one from the casing tripping operation. However, there exists a minimum mud density, below which the horizontal OHEC under the combined operation will significantly decrease. This minimum density is jointly controlled by the casing pulling operation and the POOH operation. The recommended mud density ranges from $\rho_{m-com-min}$ to $\rho_{m-com-optimal}$ (see Fig. 3(d)).

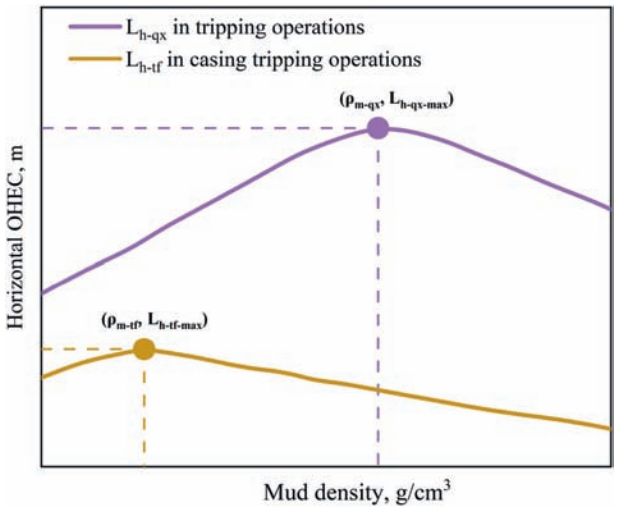


Fig. 2. Horizontal OHEC under different scenarios without intersection.

In field conditions, the large diameter of the casing results small annular space lead to significant axial pressure fluctuations during casing tripping operations. This causes the horizontal OHEC under casing tripping to be significantly lower than that under the tripping operations. Additionally, the casing running speed is generally higher than the casing pulling speed, exacerbating pressure fluctuations during casing running. Consequently, the optimal mud density for casing tripping operations is typically lower than that for tripping operations, and the optimal mud density for combined operations is usually smaller than that for tripping operations alone.

In practical operations, due to the combined effects of the above factors, the horizontal OHEC under the combined operation is most often observed to follow scenario b. To determine the optimal mud density for the combined operation, further detailed analysis is needed. By solving the system of equations from Equation (13) and Equation (19), the optimal density can be obtained:

$$\frac{\left(D_o - D_{dp}\right)\left[\rho_m - \max(\rho_c, \rho_p)\right]}{f_{qz} v_{qz}^2} = \frac{\left(D_o - D_{cp}\right)\left(\rho_f - \rho_m\right)}{f_{xf} v_{xf}^2} \tag{27}$$

By solving the system of equations from Equation (6), Equation (7), and Equation (26), which can be obtained:

$$\begin{cases} \dfrac{\rho_m - \max(\rho_c, \rho_p)}{\rho_f - \rho_m} = \left(\dfrac{D_o - D_{cp}}{D_o - D_{dp}}\right)^{n+1} \left(\dfrac{v_{xf}}{v_{qz}}\right)^{-n} \ (\mathrm{Re} \le 2100) \\ \dfrac{\rho_m - \max(\rho_c, \rho_p)}{\rho_f - \rho_m} = \left(\dfrac{D_o - D_{cp}}{D_o - D_{dp}}\right)^{nb+1} \left(\dfrac{v_{xf}}{v_{qz}}\right)^{2b-nb-2}, \\ b = 0.25 - 0.143 \lg n \ (\mathrm{Re} > 2100) \end{cases} \tag{28}$$

The optimal mud density under the combined conditions is:

$$\rho_{m-com} = \begin{cases} \rho_f - \dfrac{\rho_f - \max(\rho_c, \rho_p)}{\left(\dfrac{D_o - D_{cp}}{D_o - D_{dp}}\right)^{n+1} \left(\dfrac{v_{xf}}{v_{qz}}\right)^{-n} + 1} \ (\mathrm{Re} \le 2100) \\ \rho_f - \dfrac{\rho_f - \max(\rho_c, \rho_p)}{\left(\dfrac{D_o - D_{cp}}{D_o - D_{dp}}\right)^{nb+1} \left(\dfrac{v_{xf}}{v_{qz}}\right)^{2b-nb-2} + 1}, \\ b = 0.25 - 0.143 \lg n \ (\mathrm{Re} > 2100) \end{cases} \tag{29}$$

3. Application examples

3.1. Calculation of horizontal OHEC and the optimal mud density

A calculation and analysis of the horizontal OHEC and optimal mud density for a ERHW in the South China Sea oil field was conducted. The main data for the wellbore structure and drilling parameters of this ERHW are shown in Fig. 4 and Table 1.

The horizontal OHEC variation with mud density was analyzed during drilling, tripping and casing tripping operations (see Fig. 5), the horizontal OHEC under tripping conditions initially increases and then decreases with increasing mud density. This trend is due to the cooperative effects of mud density on RIH and POOH processes: higher mud density increases bottomhole pressure during RIH, reducing horizontal OHEC by increasing wellbore fracture risk, while it enhances horizontal OHEC during POOH by

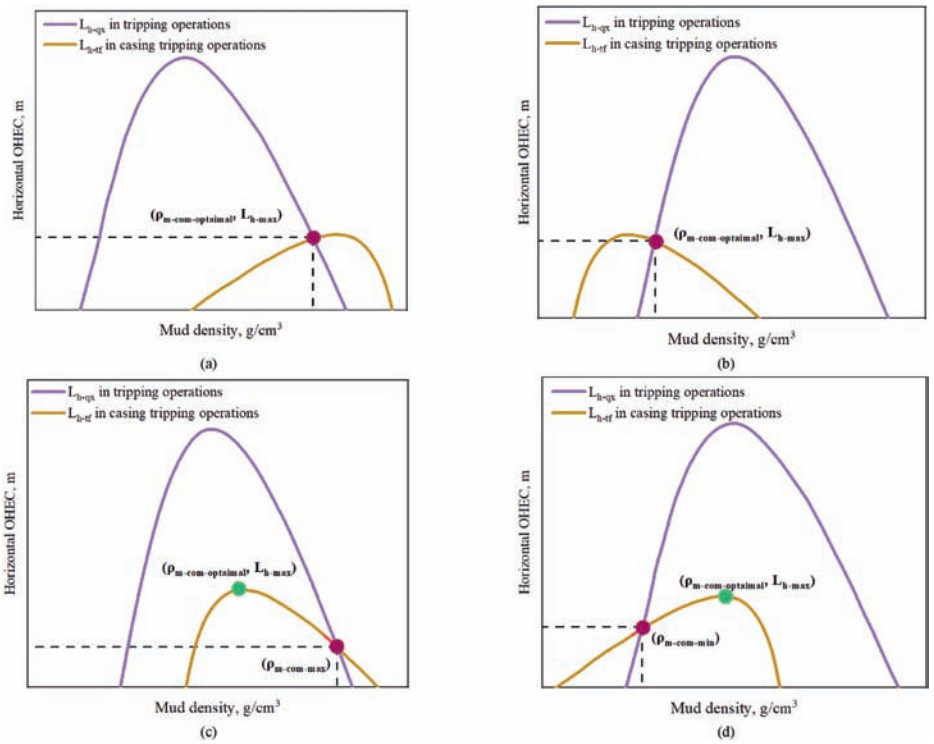


Fig. 3. Horizontal OHEC under different intersection scenarios.

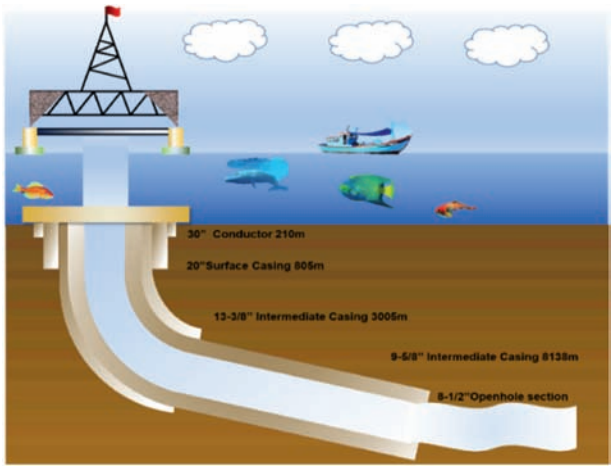


Fig. 4. Wellbore structure and wellbore trajectory diagram.

Table 1
Drilling parameters.

Parameters	Values
Borehole vertical depth/m	1956
Consistency coefficient/(Pa·s^n)	0.39
Mud flow rate/(L/s^{-1})	30
Liquidity index	0.65
Mud density/(g·cm^{-3})	1.25
Fracture pressure equivalent density/(g·cm^{-3})	1.81
Pore pressure equivalent density/(g·cm^{-3})	1.01
Collapse pressure equivalent density/(g·cm^{-3})	1.05
Casing pulling speed/(m·s^{-1})	0.15
Casing running speed/(m·s^{-1})	0.3
POOH speed/(m·s^{-1})	0.6
RIH speed/(m·s^{-1})	0.8
Drill string diameter/mm	127
Rate of penetration (ROP)/(m·h^{-1})	10
Drilling string rotation speed/rpm	100

decreasing wellbore collapse risk. Thus, an optimal mud density exists for maximum horizontal OHEC under tripping conditions. When the mud density exceeds this critical value, the horizontal OHEC under tripping conditions is controlled by the RIH process. Similarly, the horizontal OHEC under casing tripping conditions follows the same trend.

Analytical calculations show that without considering string tripping conditions, the horizontal OHEC peaks at 2334 m with a mud density of 1.28 g/cm^3. However, when string tripping is considered, the maximum horizontal OHEC is 1865 m at 1.33 g/cm^3 during tripping conditions and the maximum OHEC is 1693 m at 1.29 g/cm^3 during casing tripping conditions. For accurate prediction, both drilling and string tripping conditions must be considered. Ignoring string tripping pressure fluctuations can lead to significant errors in OHEC prediction. The intersection of tripping and casing tripping conditions represents the maximum OHEC under combined scenarios, with an optimal mud density of 1.302 g/cm^3 and a maximum OHEC of 1605 m. This value falls within the SMWW. Notably, different string tripping speeds can influence the optimal mud density to varying extents.

3.2. Comparison of measured downhole fluctuating pressure with predicted results

As shown in Fig. 6, we compare the predicted pressure fluctuations with the actual measured pressure fluctuations and demonstrate the variations at different depths. The error between the predicted and measured downhole pressure fluctuations is within 10%, which is within the acceptable engineering error. The

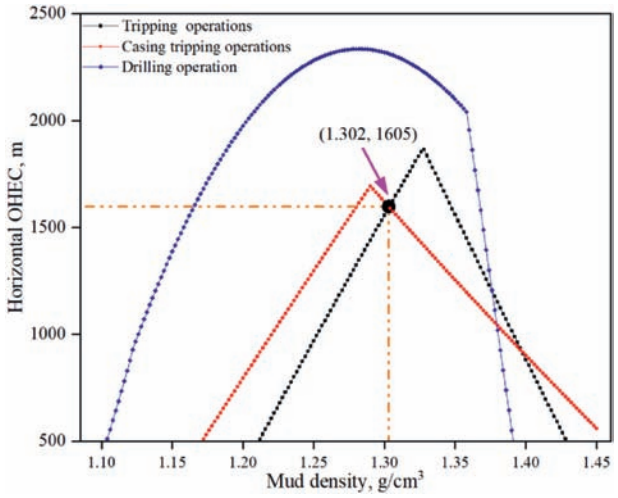


Fig. 5. Horizontal OHEC controlled by combined operating conditions.

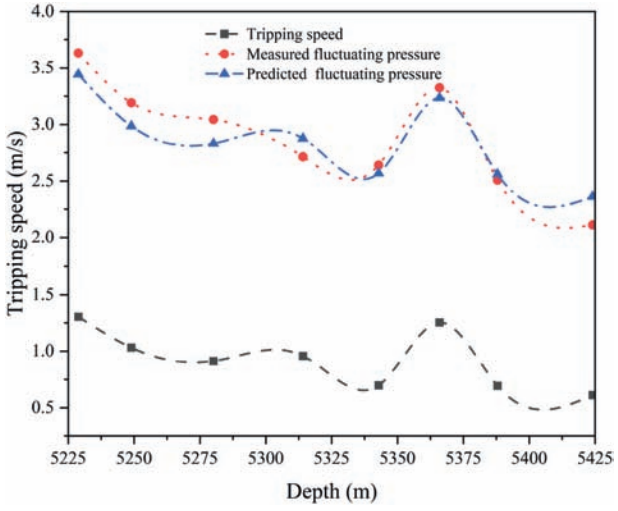


Fig. 6. Measured and predicted verification analysis of bottomhole pressure during tripping operations.

results show that the model predictions align well with the actual measurement data, further validating the accuracy of our model. Additionally, we have incorporated tripping speeds to illustrate their relationship with the pressure fluctuations.

4. Correlation analysis

4.1. Sensitivity analysis of horizontal OHEC during drilling operations

4.1.1. The effects of mud density and flow rate on horizontal OHEC under drilling operation

As shown in Fig. 7, it can be observed that, at a constant mud density, the horizontal OHEC first increases and then decreases with an increase in mud flow rate. This is because, during the drilling process, increasing the mud flow rate reduces the thickness of the cuttings bed, thereby lowering the annular pressure loss. However, when the thickness of the cuttings bed decreases to a point where it no longer significantly affects the mud circulation efficiency, further increasing the mud flow rate leads to a sharp

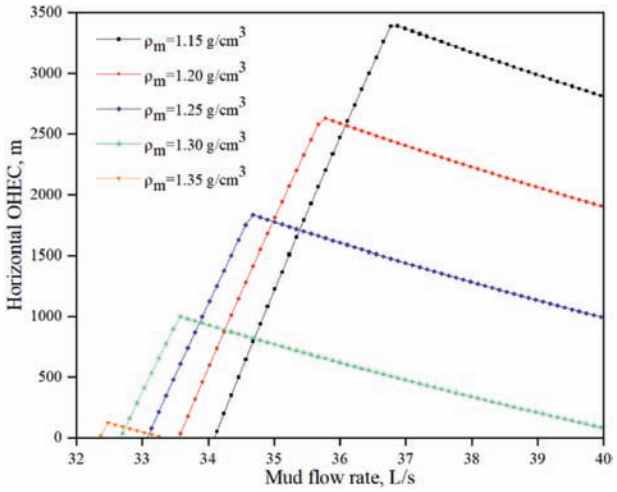


Fig. 7. Variations of horizontal OHEC with mud flow rate at different mud density values.

rise in annular pressure loss, which in turn leads to a decrease in the horizontal OHEC. Specifically, as the mud density increases, the horizontal OHEC generally shows a decreasing trend. Particularly under high-density conditions (such as 1.35 g/cm^3), the horizontal OHEC is almost zero.

4.1.2. The effects of ROP and drill string rotational speed on horizontal OHEC under drilling operation

As shown in Fig. 8, the horizontal OHEC significantly increases with increasing drill string rotational speed. This increase is attributed to the effective disruption of the cuttings bed by the rotating drill string, which reduces annular pressure loss. However, the enhancement of horizontal OHEC plateaus beyond a certain rotational speed. For instance, at a ROP of 5 m/h, the horizontal OHEC ceases to increase when the drill string speed exceeds 87 rpm. Excessively high rotational speeds can also challenge the surface rig's torque capacity. Additionally, as ROP increases, higher drill string speeds are required to prevent excessive cuttings accumulation. For example, to achieve optimal horizontal OHEC, the drill string speed must increase from 87 rpm to 96 rpm when the ROP increases from 5 m/h to 10 m/h.

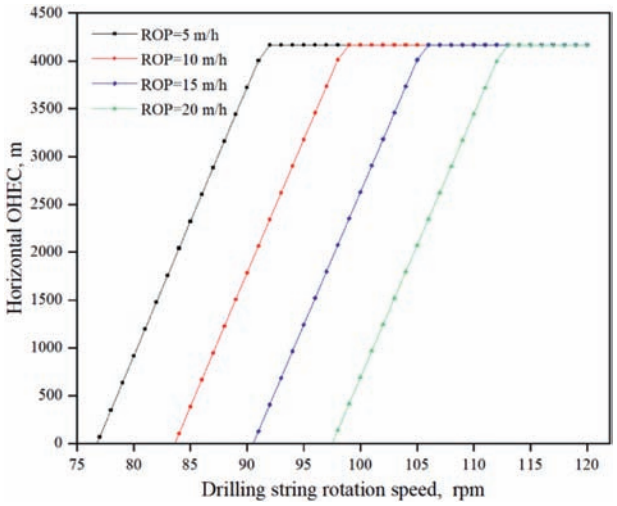


Fig. 8. Variations of horizontal OHEC with drill string rotational speed at different ROP values.

4.2. Sensitivity analysis of horizontal OHEC under string tripping operations

4.2.1. The effects of mud density and string tripping speed on horizontal OHEC under string tripping operations

Surge pressures during RIH can induce wellbore fracturing, whereas suction pressures during POOH may cause wellbore collapse. For a designed horizontal section length of 1500 m and a mud density of 1.25 g/cm^3, the maximum safe string tripping speeds are as follows: RIH speed, 1.36 m/s (see Fig. 9(a)); POOH speed, 0.89 m/s (see Fig. 9(b)); casing running speed, 0.58 m/s (see Fig. 9(c)); and casing pulling speed, 0.21 m/s (see Fig. 9(d)). Tripping speeds should not exceed these maximum safe values to ensure wellbore stability. If field operations require increasing the casing pulling speed to 0.3 m/s, the mud density must be adjusted to 1.30 g/cm^3 to maintain the design requirements for the horizontal section length. Additionally, when the tripping speed increases, the fluid flow in certain sections of the wellbore may transition from laminar to turbulent flow, leading to a reduction in annular pressure loss, a decrease in bottom-hole pressure, and an increase in OHEC. The interaction between different pipe column compositions in multi-layered pipe strings may cause a temporary "jump" in OHEC at specific points, followed by a return to a stable turbulent flow state. After three such jumps, the fluid in the annulus will stabilize into a fully turbulent state.

4.2.2. The effects of mud flow behavior index and consistency coefficient on **horizontal OHEC** under casing tripping operations

As shown in Fig. 10, the horizontal OHEC decreases significantly with increasing consistency coefficient when the flow behavior index of the mud is fixed. For casing tripping conditions, simulations reveal that at a casing pulling speed of 0.6 m/s and a designed horizontal section length of 1500 m, a flow behavior index of 0.6 and a consistency coefficient of 0.1 just meet the casing pulling requirements (see Fig. 10(d)). To improve this, the casing pulling speed can be reduced, or the mud rheological property can be adjusted. Specifically, lowering the flow behavior index to below 0.58 and increasing the consistency coefficient to 0.52 can stabilize the open-hole wellbore during casing pulling. Therefore, during tripping operations, the mud rheological properties should be adjusted in real-time based on downhole conditions to ensure the string reaches the designed measured depth.

4.2.3. The effect of drilling assembly on horizontal OHEC under string tripping operations

As shown in Fig. 11, the field-used drilling assembly is 5000 m 5–7/8″ and 5″ drill strings. During POOH operations at 0.95 m/s, the horizontal OHEC is 927 m. Adjusting the assembly to 3000 m of 5–7/8″ drill string plus 5″ drill string allows meeting the required tripping speed while satisfying the design requirements for the 1500 m horizontal section. During casing tripping, drilling assembly adjustments have minimal impact on horizontal OHEC, as pressure fluctuations and annular losses are primarily associated with lowering the liner in the horizontal section. For a designed horizontal section length of 1500 m (using a 5160 m 5–7/8″ heavy drill string, 2983 m 5″ drill string and 7" liner), the casing running speed should not exceed 0.57 m/s, and the casing pulling speed should not exceed 0.21 m/s.

4.3. Sensitivity analysis of optimal mud density under combined operations

4.3.1. Variation trends of optimal mud density under combined operations with changes to POOH and casing running speed

As shown in Fig. 12, the optimal mud density under combined conditions is influenced by casing running speed and POOH speed. When casing running speed is constant, the optimal mud density decreases with increasing POOH speed. Conversely, when POOH speed is constant, the optimal mud density increases with casing running speed, with the increasing trend gradually slowing down. This is due to the reduction in horizontal OHEC caused by

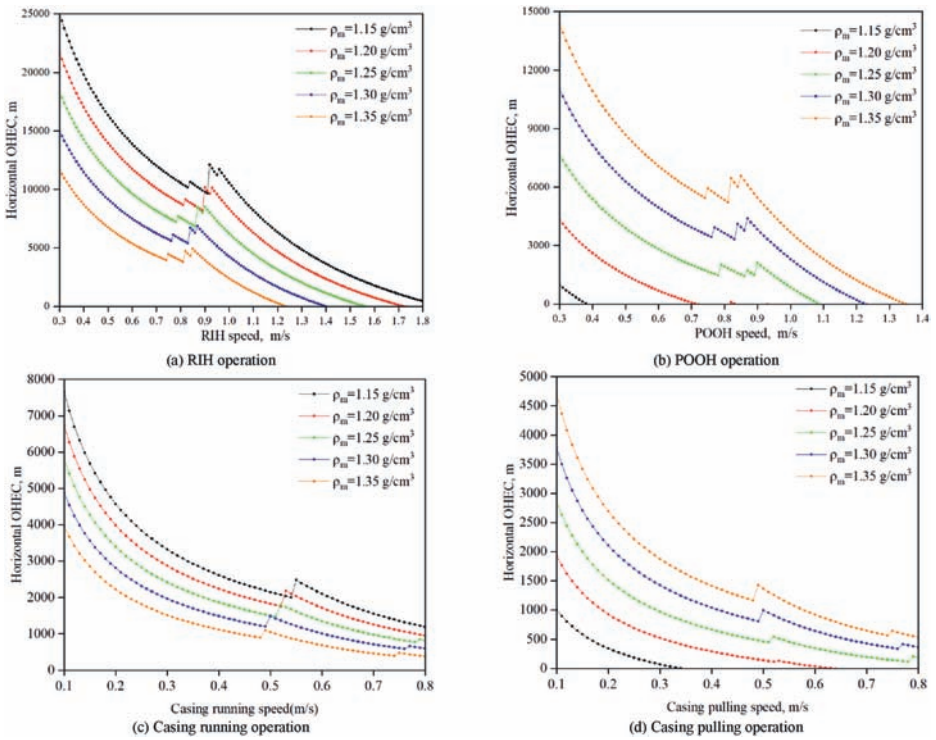


Fig. 9. Variations of horizontal OHEC with string tripping speed under different mud density values.

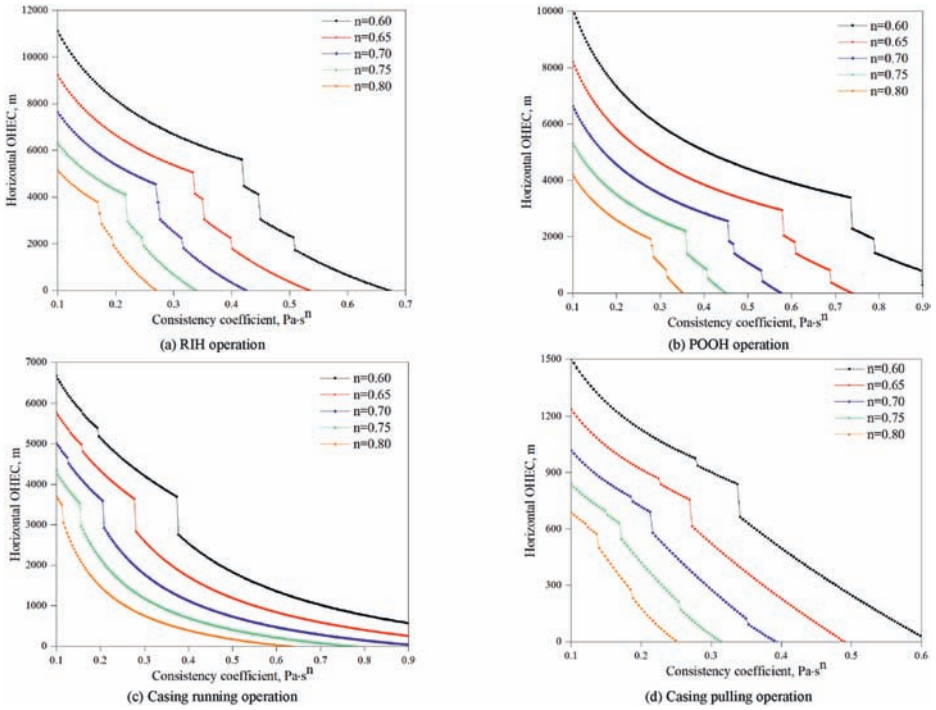


Fig. 10. Variations of horizontal OHEC with consistency coefficient at different flow behavior index values under string tripping operations.

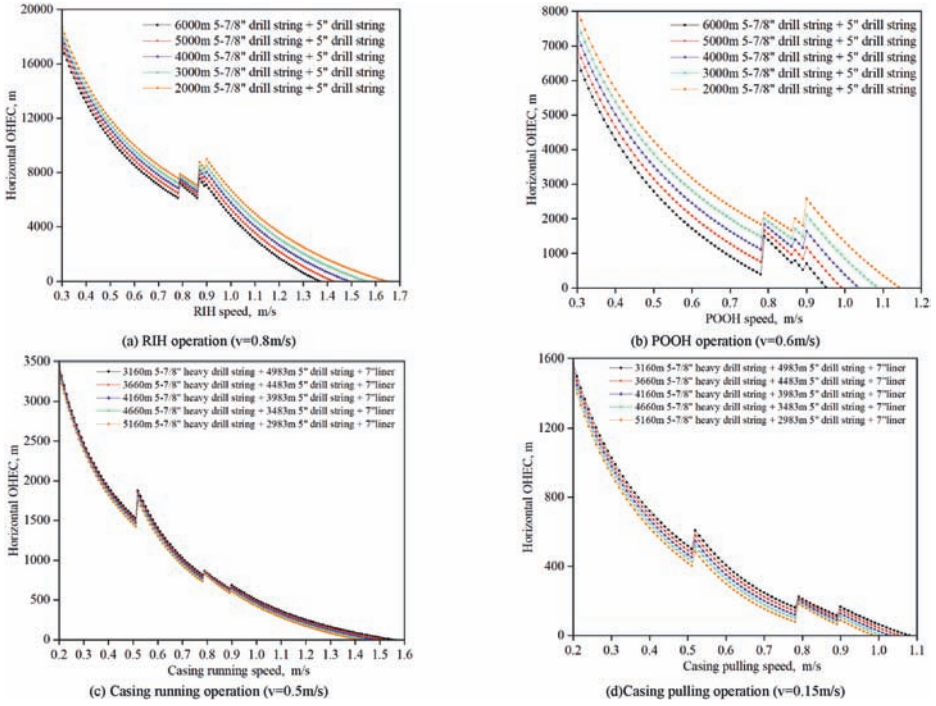


Fig. 11. Variations of horizontal OHEC with string tripping speed under different drilling assembly.

increased casing running speed, which shifts the intersection point of horizontal OHEC for both conditions and results in a higher optimal mud density. At relatively low POOH speeds, the optimal mud density exhibits an upward concave trend as casing running speed increases.

4.3.2. Variation trends of optimal mud density under combined operations with measurement uncertainties to collapse pressure、pore pressure and fracture pressure

As shown in Fig. 13, to evaluate the impact of measurement uncertainties in formation properties on the optimal mud density,

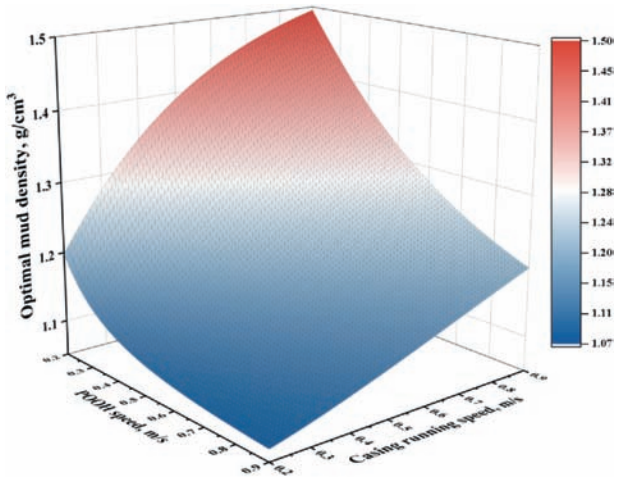


Fig. 12. Variation trends of optimal mud density with POOH speed and casing running speed under combined conditions.

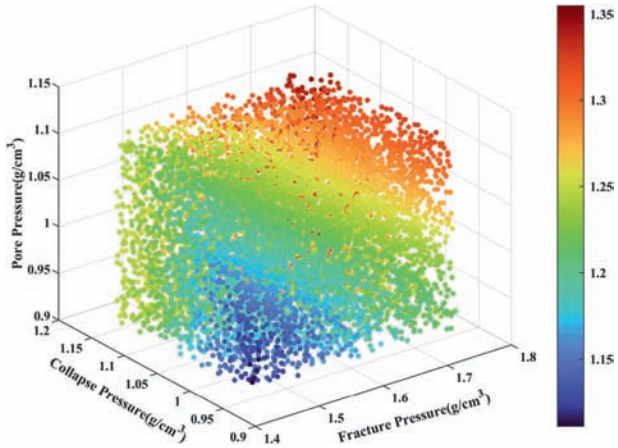


Fig. 13. Optimal mud density considering the uncertainties of fracture pressure, collapse pressure, and pore pressure.

we conducted a sensitivity analysis using Monte Carlo simulations (Opoku et al., 2020; Williamson et al., 2006). A total of 1000 simulations were performed to assess the effects of uncertainties in fracture pressure, pore pressure, and collapse pressure. The simulation results showed that the optimal mud density averaged 1.2447 g/cm^3 with a standard deviation of 0.0454, indicating that the values were tightly concentrated around the mean.

As shown in Fig. 14, the sensitivity analysis revealed that fracture pressure and collapse pressure are the most influential parameters on the optimal mud density, with Spearman correlation coefficients of 0.66246 and 0.59541, respectively. These pressures exhibited a strong positive correlation with the optimal mud density, on the other hand, pore pressure showed a weaker influence, with a Spearman correlation coefficient of 0.27399.

4.3.3. Variation trends of optimal mud density under combined operations with changes to POOH speed and changes in wellbore, casing, and drill string diameter

As shown in Fig. 15(a)–(c), the optimal mud density under combined conditions increases with POOH speed when the diameters of wellbore, casing, and drill string are fixed, exhibiting a convex upward trend. This trend is driven by the increasing horizontal OHEC under POOH conditions with mud density. However, as POOH speed rises, the rate of increase in horizontal OHEC slows, shifting the intersection point of combined conditions to higher mud densities. When POOH speed is fixed, the optimal mud density under combined conditions also increases with an increase in wellbore diameter, a decrease in casing diameter, or an increase in drill string diameter, albeit at a lower rate. This is attributed to the reduced annular pressure loss resulting from the increased outer diameter of the annulus. As mud density rises, the horizontal OHEC under POOH conditions increases more rapidly than under casing running conditions, where the rate of increase slows, shifting the intersection point of combined conditions.

4.3.4. Variations trend of optimal mud density under combined conditions with changes to casing running speed and changes in wellbore, casing, and drill string diameter

As shown in Fig. 15(d)–(f), the optimal mud density under combined conditions decreases with increasing casing running speed when the diameters of wellbore, casing, and drill string are

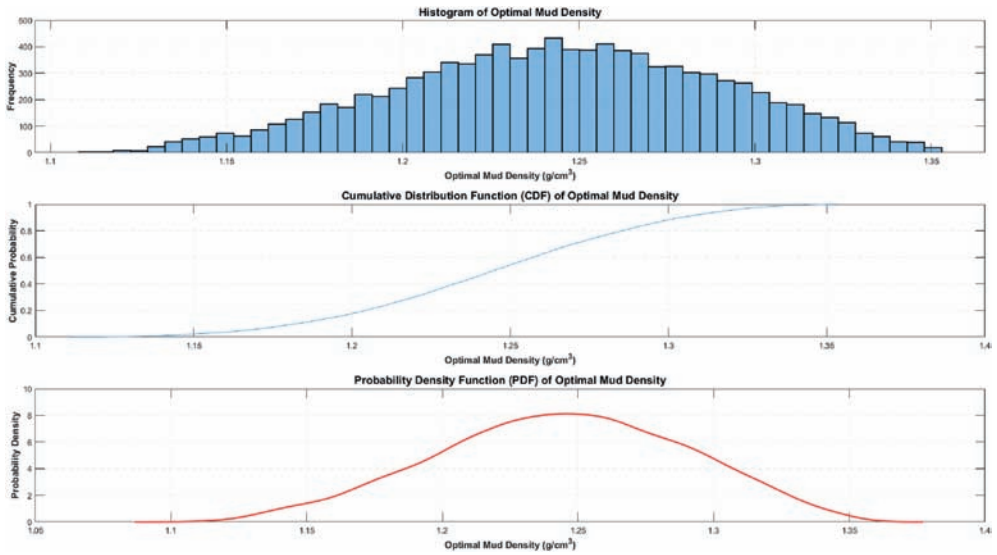


Fig. 14. Statistical analysis of optimal mud density: Histogram, CDF, and PDF.

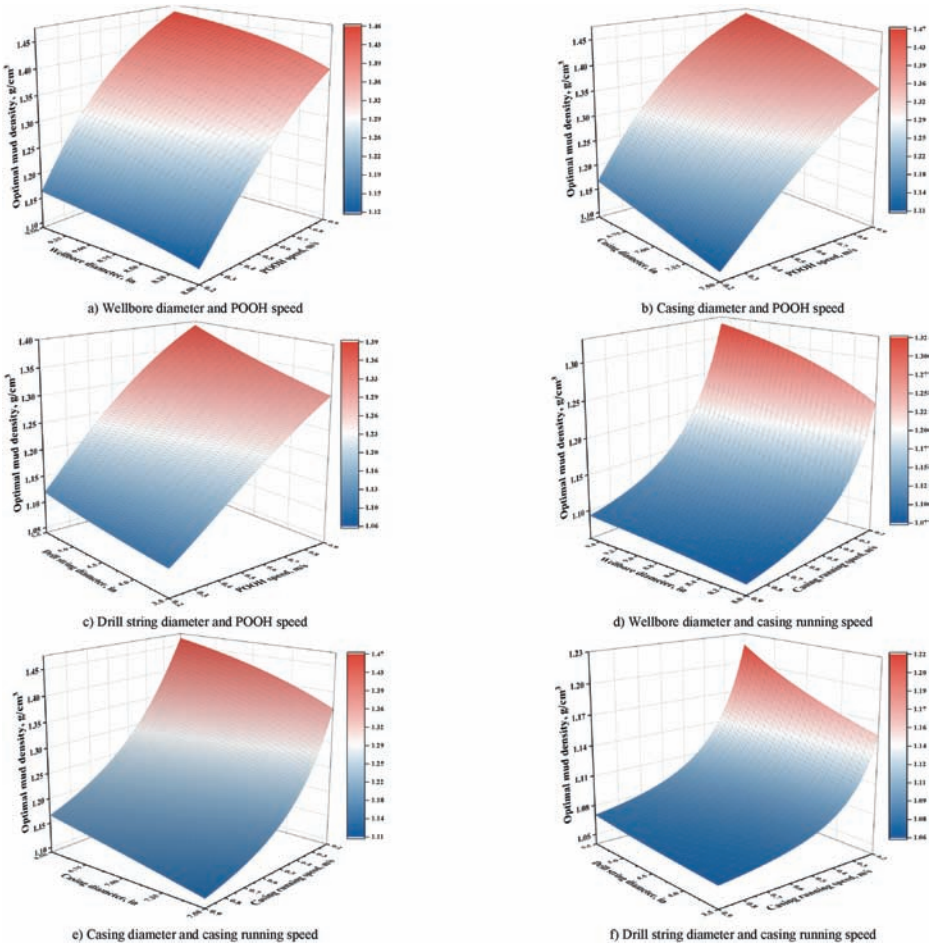


Fig. 15. Variation trends of optimal mud density with multiple factors under combined operations.

fixed, exhibiting a concave upward trend. This decrease is due to the reduction in horizontal OHEC under casing running conditions, which shifts the intersection point of the two conditions to lower mud densities. The rate of decrease in optimal mud density slows with further increases in casing running speed, and the optimal horizontal OHEC also decreases. When the casing running speed is fixed, the optimal mud density under combined conditions increases with an increase in wellbore and drill string diameters and a decrease in casing diameter. This trend is attributed to the reduced annular pressure loss resulting from the increased outer diameter of the annulus. However, the rate of increase in optimal mud density slows as these dimension change.

4.3.5. *Variation trends of optimal mud density with changes to drill string diameter under combined operating conditions*

As shown in Fig. 16, variations in casing, wellbore, and drill string diameters significantly influence the optimal mud density. An increase in casing diameter reduces the annular space gap, sharply decreasing the horizontal OHEC under casing running conditions and shifting the optimal mud density to a lower value. Changes in casing diameter have a particularly pronounced effect on optimal mud density. With the increasing in drill string diameter reduces the horizontal OHEC under POOH conditions, also shifting the optimal mud density to a lower value. Conversely, an increase in wellbore diameter widens the annular space gap,

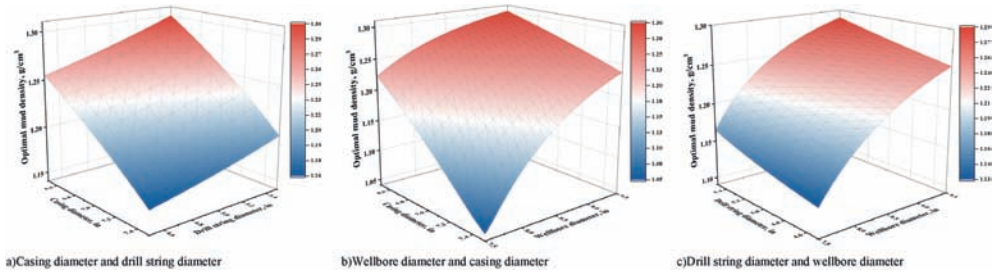


Fig. 16. Variation trends of optimal mud density with string dimensions under combined operations.

enhancing the horizontal OHEC for both tripping and casing running conditions. However, the improvement in horizontal OHEC is more significant under casing running conditions, resulting in a lower optimal mud density. All in all, considering the combined effects of casing, wellbore, and drill string diameters, appropriate adjustments to mud density can effectively prevent formation fracture and wellbore collapse, ensuring drilling safety.

5. Conclusions

(1) An optimal mud density model in ERHD was established based on the prediction and analysis of horizontal OHEC of ERHWs under string tripping operations. The analysis revealed that the horizontal OHEC initially increases and subsequently decreases with increasing mud density for both tripping and casing tripping operations. Each operation exhibits an optimal mud density that maximizes the OHEC of horizontal ERHWs.
(2) Under combined operating conditions, the optimal mud density can be categorized into two primary scenarios: In the first scenario, the OHEC curves for tripping and casing tripping operations do not intersect, and the optimal mud density is determined solely by casing tripping operations. In the second scenario, the OHEC curves intersect, resulting in four subcases. In two subcases, the optimal mud density is influenced by both tripping and casing tripping operations, whereas in the remaining two subcases, it is dictated exclusively by casing tripping operations.
(3) The optimal mud density is positively correlated with POOH speed, wellbore diameter and drill string diameter. Conversely, it is negatively correlated with casing diameter and casing running speed.
(4) Considering the uncertainties in the geological mechanical parameters, the optimal mud density is positively correlated with fracture pressure and collapse pressure, with sensitivity decreasing in the order of fracture pressure, collapse pressure, and pore pressure.
(5) It is important to note that the optimal mud density model has a certain range of applicability. The likelihood of encountering transitional flow during ERHD is low, and in this study, we assume that the mud flow is in a turbulent state. Additionally, the model does not account for the effects of formation heterogeneity and anisotropy along the horizontal section.

CRediT authorship contribution statement

Xuyue Chen: Investigation, Conceptualization, Methodology, Writing-original draft, Writing-review & editing, Funding acquisition, Supervision. **Gengchen Li:** Investigation, Methodology, Visualization, Validation, Formal analysis, Writing-original draft, Writing-review & editing. **Qiqi Yang:** Investigation, Methodology, Visualization. **Jin Yang:** Conceptualization, Supervision. **Deli Gao:** Conceptualization, Supervision. **Qinyi He:** Investigation, Methodology.

Acknowledgments

This work was financially supported by the National Natural Science Foundation of China (Grant numbers: 52174012; 52394250; 52394255; 52234002; U22B20126; 51804322), Ministry of Industry and Information Technology High-tech Ship Scientific Research Project (CBG2N21-4).

Nomenclature

a,b	The empirical coefficients dependent on the fluidity index of the mud, dimensionless
C_s	The solid volumetric concentration, %
D_{cp}	The outer diameter of the casing, mm
D_{dp}	The outer diameter of the drill string, mm
D_0	The outer diameter of the annulus, mm
D_v	The vertical depth of the target level, m
f_{qz}	The friction coefficient in the annulus during POOH operation, dimensionless
f_{st}	The dimensionless annular friction coefficient during casing pulling operation
f_{xf}	The dimensionless annular friction coefficient during casing running operation
f_{xz}	The friction coefficient in the annulus during RIH operation, dimensionless
g	The acceleration due to gravity, N/kg
k	The consistency coefficient, Pa·s^n
L_{di}	The length of the inclined section of the borehole, m
$L_{\mathrm{h}-qx}$	The horizontal OHEC during tripping operation, m
$L_{\mathrm{h}-tf}$	The horizontal OHEC during casing tripping operations, m
L_{dri}	The horizontal OHEC during drilling operation, m
L_{v}	The length of the vertical section of the borehole, m
n	The liquidity index, dimensionless
Δp_{h-qz}	The suction pressure in the horizontal section during tripping operation, MPa
Δp_{h-xz}	The surge pressure in the horizontal section during tripping operation, MPa
Δp_a	Total annular pressure drop, MPa
$(\Delta p/\Delta L)_h$	The pressure loss gradients in horizontal section, MPa/m
p_{sc}	The suction pressure, MPa
p_{sx}	The surge pressure, MPa
Re_{qz}	The Reynolds number of the mud during POOH operation, dimensionless
Re_{xz}	The Reynolds number of the mud during RIH operation, dimensionless
v_{ph}	The POOH speed, m/s
v_{qz}	The flow velocity of the mud in the annulus during POOH, m/s
v_{rh}	The RIH speed, m/s
v_{st}	The annular mud velocity during casing pulling operation, m/s
v_{xf}	The annular drilling mud velocity during casing running operation, m/s
v_{xz}	The flow velocity of the drilling mud in the annulus during RIH operation, m/s
ΔP_{st}	The suction pressure under casing pulling operation, MPa
ΔP_{xf}	The surge pressure under casing running operation, MPa
ρ_c	The collapse pressure equivalent density, g/cm^3
ρ_f	The fracture pressure equivalent density, g/cm^3
ρ_m	The mud density, g/cm^3
ρ_{m-tf}	The optimal mud density during casing tripping operations, g/cm^3
ρ_{m-qx}	The optimal mud density during tripping operations, g/cm^3
ρ_p	The pore pressure equivalent density, g/cm^3
$\rho_{\mathrm{m-com-optimal}}$	The optimal mud density under the combined operations, g/cm^3

References

Chen, X., Gao, D., 2016. Mega-extended-reach drilling to deepwater target: what is the well's maximum allowable measured depth while drilling?. In: SPE International Petroleum Exhibition & Conference Abu Dhabi. UAE. https://doi.org/10.2118/183025-ms. SPE-183025-MS.

Chen, X., Gao, D., 2018. The maximum-allowable well depth while performing ultra-extended-reach drilling from shallow water to deepwater target. SPE J. 23 (1), 224–236. https://doi.org/10.2118/183025-Pa.

Chen, X., Du, X., Yang, J., Gao, D., Zou, Y., He, Q., 2022. Developing offshore natural gas hydrate from existing oil & gas platform based on a novel multilateral wells system: depressurization combined with thermal flooding by utilizing geothermal heat from existing oil & gas wellbore. Energy 258, 124870. https://doi.org/10.1016/j.energy.2022.124870.

Chen, X., Wang, R., Yang, J., Gao, D., Li, G., Li, P., 2025. A new intelligent optimization method for drilling parameters of extended reach wells based on mechanical specific energy and machine learning. Petrol. Res. 10 (3), 485–500. https://doi.org/10.1016/j.ptlrs.2025.03.002.

Chen, X., Yang, J., Gao, D., Hong, Y., Zou, Y., Du, X., 2020. Unlocking the deepwater natural gas hydrate's commercial potential with extended reach wells from shallow water: review and an innovative method. Renew. Sustain. Energy Rev. 134, 110388. https://doi.org/10.1016/j.rser.2020.110388.

Fan, H., 2014. Practical Drilling Fluid Mechanics. Petroleum Industry Press, Beijing.

Gao, D., Huang, W., Li, X., 2019. Research on extension limits and engineering design methods for extended reach drilling. Petrol Drill Technol. 47 (3), 1–8. https://doi.org/10.11911/syztjs.2019069 (In Chinese).

Gao, D., Tan, C., Tang, H., 2009. Limit analysis of extended reach drilling in South China Sea. Pet. Sci. 6 (2), 166–171. https://doi.org/10.1007/s12182-009-0026-8.

He, S., Tang, M., Xiong, J., Wang, W., 2016. A numerical model to predict surge and swab pressures for yield power law fluid in concentric annuli with open-ended pipe. J. Pet. Sci. Eng. 145, 464–472. https://doi.org/10.1016/j.petrol.2016.05.039.

Huang, W., Gao, D., Wei, S., Chen, P., 2015. Boundary conditions: a key factor in tubular-string buckling. SPE J. 20 (6), 1409–1420. https://doi.org/10.2118/174087-pa.

Islam, R., Khan, F., Venkatesan, R., 2017. Real time risk analysis of kick detection: testing and validation. Reliab. Eng. Syst. Saf. 161, 25–37. https://doi.org/10.1016/j.ress.2016.12.014.

Lan, P., Polychronopoulou, K., Iaccino, L.L., Bao, X., Polycarpou, A.A., 2018. Elevated-temperature and -Pressure tribology of drilling fluids used in oil and gas extended-reach-drilling applications. SPE J. 23 (6), 2339–2350. https://doi.org/10.2118/191380-pa.

Li, G., Wang, L., Li, Q., Yang, X., 2024. Research and practice on optimization methods for drilling parameters and drilling fluid performance of extended reach Wells based on wellbore cleaning effect. Offshore Oil 44 (2), 94–99. https://doi.org/10.3969/j.issn.1008-2336.2024.02.094.

Li, W., Xia, Y., Chen, X., Chen, H., Li, Y.M., Li, X.Q., 2020. Research and application of downhole blowout prevention system while drilling: a review. J. Pet. Sci. Eng. 188, 106882. https://doi.org/10.1016/j.petrol.2019.106882.

Li, X., Gao, D., Chen, X., 2017a. A comprehensive prediction model of hydraulic extended-reach limit considering the allowable range of drilling fluid flow rate in horizontal drilling. Sci. Rep. 7 (1), 3083. https://doi.org/10.1038/s41598-017-03261-3.

Li, X., Gao, D., Zhou, Y., Zhang, H., Yang, Y., 2017b. Study on the prediction model of the open-hole extended-reach limit in horizontal drilling considering the effects of cuttings. J. Nat. Gas Sci. Eng. 40, 159–167. https://doi.org/10.1016/j.jngse.2017.02.013.

Li, Z., Zhang, J., Xing, X., Hu, P., Kamgue Lenwoue, A.R., Zhang, Y., Tong, G., 2022. Influence of drill string size on hydraulic elongation limit of extended reach wells-taking well X in Bohai oilfield as an example. Arab J. Sci. Eng. 47 (9), 12031–12043. https://doi.org/10.1007/s13369-022-06830-5.

Livescu, S., Craig, S., Watkins, T., 2014. Challenging the industry's understanding of the mechanical friction reduction for coiled tubing operations. In: SPE Annual Technical Conference and Exhibition. https://doi.org/10.2118/170635-ms. Amsterdam, The Netherlands. SPE-170635-MS.

Mason, C.J., Judzis, A., 1998. Extended-reach drilling – what is the limit?. In: SPE Annual Technical Conference and Exhibition. New Orleans, Louisiana. https://doi.org/10.2118/48943-ms. SPE-48943-MS.

Melikoglu, M., 2018. Current status and future of ocean energy sources: a global review. Ocean Eng. 148, 563–573. https://doi.org/10.1016/j.oceaneng.2017.11.045.

Opoku, D., Al-Ghamdi, A., Osei, A., 2020. Novel method to estimate bottom hole pressure in multiphase flow using quasi-Monte Carlo method. In: International Petroleum Technology Conference. https://doi.org/10.2523/IPTC-20080-MS. Dhahran, Saudi Arabia.

Rocha, L.A.S., Andrade, R., Soffried, K., 2003a. How water depth affects extended reach drilling. In: Offshore Technology Conference. https://doi.org/10.4043/15326-ms. Houston, Texas, U.S.A. SPE-15326-MS.

Rocha, L.A.S., Junqueira, P., Roque, J.L., 2003b. Overcoming deep and ultra deep-water drilling challenges. In: Offshore Technology Conference. https://doi.org/10.4043/15233-ms. Houston, Texas, U.S.A. SPE-15233-MS.

Shi, X., Huang, W., Gao, D., Zhu, N., Li, W., 2023. Extension limit analysis of drill-string with drag reduction oscillators in horizontal drilling. Geoenergy Sci. Eng. 228, 211996. https://doi.org/10.1016/j.geoen.2023.211996.

Siddiqi, F.A., Riskiawan, A., Al-Yami, A., Elmarsafawi, Y., Jain, B., Louati, I., Martanto, R., Taoutaou, S., 2016. Successful managed pressure cementing with hydraulic simulations verification in a narrow pore-frac pressure window using managed pressure drilling in Saudi Arabia. In: SPE Annual Technical Conference and Exhibition, Dubai. UAE. https://doi.org/10.2118/182500-ms. SPE-182500-MS.

Song, D., Honghai, F., Deqiang, T., Yuhan, L., 2016. Calculation and application of safe mud density window in deepwater shallow layers. In: Offshore Technology Conference. https://doi.org/10.4043/27063-MS. Houston, Texas, USA. SPE-27063-MS.

Suo, Y., Dong, M., Fu, X., He, W., Pan, Z., 2024. Experimental and numerical simulation research on hot dry rock wellbore stability under different cooling methods. Geothermics 119, 102977. https://doi.org/10.1016/j.geothermics.2024.102977.

Tang, M., Ahmed, R., Srivastav, R., He, S., 2016. Simplified surge pressure model for yield power law fluid in eccentric annuli. J. Pet. Sci. Eng. 145, 346–356. https://doi.org/10.1016/j.petrol.2016.05.038.

Wada, R., Kaneko, T., Ozaki, M., Inoue, T., Senga, H., 2018. Longitudinal natural vibration of ultra-long drill string during offshore drilling. Ocean Eng. 156, 1–13. https://doi.org/10.1016/j.oceaneng.2018.02.054.

Wang, X., Zhang, F., Wang, X., Yu, Y., Lou, W., Peng, F., 2024. Evaluating the maximum drilling length of horizontal geothermal wells utilizing temperature constraints. Geoenergy Sci. Eng. 238, 212884. https://doi.org/10.1016/j.geoen.2024.212884.

Wen, Z., Wang, J., Wang, Z., He, Z., Song, C., Liu, X., Zhang, N., Ji, T., 2023. Analysis of the world deepwater oil and gas exploration situation. Petrol. Explor. Dev. 50 (5), 1060–1076. https://doi.org/10.1016/s1876-3804(23)60449-5.

Williamson, H.S., Sawaryn, S.J., Morrison, J.W., 2006. Monte Carlo techniques applied to well forecasting: some pitfalls. SPE Drill. Complet. 21 (3), 216–227. https://doi.org/10.2118/89984-PA.

Willson, S.M., Edwards, S., Heppard, P.D., Li, X., Coltrin, G., Chester, D.K., Harrison, H.L., Cocales, B.W., 2003. Wellbore stability challenges in the deep water, Gulf of Mexico: case history examples from the pompano field. In: SPE Annual Technical Conference and Exhibition. https://doi.org/10.2118/84266-ms. Denver, Colorado, U.S.A. SPE-84266-MS.

Xu, J., Hong, Y., Chen, X., Zou, Y., Sun, L., Xie, T., Wang, W., 2020. What is the horizontal section's maximum allowable length during tripping or running casing in the horizontal extended-reach well. In: International Ocean and Polar Engineering Conference. Shanghai, China.

Yin, Z., Li, Z., Huang, X., 2023. Scheme optimization of deepwater dual gradient drilling based on the fuzzy comprehensive evaluation method. Ocean Eng. 281, 114978. https://doi.org/10.1016/j.oceaneng.2023.114978.

Zhang, H., Chen, Y., Wu, W., Zhang, H., Ma, D., Lu, Z., 2024. Study on open-hole extended-reach limit in horizontal drilling with wavy wellbore trajectory. Energy Sci. Eng. 12 (3), 1124–1136. https://doi.org/10.1002/ese3.1703.

Zhang, H., 2023. Status and prospect of CNOOC's extended reach well drilling technologies. Oil Drill. Prod. Technol. 45 (1), 1–11. https://doi.org/10.13639/j.odpt.2023.01.001.